JOURNAL OF GUIDANCE, CONTROL, AND DYNAMICS
Vol. 15, No. 6, November–December 1992

Analysis of Airframe and Engine Control Interactions and Integrated Flight/Propulsion Control

John D. Schierman* and David K. Schmidt†
Arizona State University, Tempe, Arizona 85287

A framework is presented for the analysis of dynamic cross-coupling between airframe and engine control systems. This approach is developed for assessing the significance of airframe/engine interactions with regard to system stability, performance, and critical frequency ranges where interactions are especially problematic. The stability robustness against airframe/engine interactions are of particular interest, and a robustness analysis approach is developed and presented. The difference between systems exhibiting two-directional vs one-directional coupling is also discussed. Two control configurations of a vehicle previously considered in several integrated flight/propulsion control studies are then evaluated using the technique, and it is shown that the baseline configuration reflects little significant airframe/engine interactions. Consequently, classical decentralized airframe and engine control laws appear to be quite adequate. However, analysis of the other system configuration shows significant performance degradation in the engine loop because of airframe/engine coupling.

Introduction

ADVANCED concepts for highly maneuverable fighter aircraft and those capable of short takeoff and vertical landing utilize the propulsion system for augmenting the lift and maneuvering capabilities of the vehicle. The integrated flight and propulsion control (IFPC) problem addressed herein and elsewhere[1-5] focuses on the interactions between airframe and engine systems, especially in control law synthesis and analysis of such configurations.

The main purpose of this paper is not to discuss any particular IFPC control law synthesis procedure but first to present an analysis framework that will expose how the interactions manifest themselves and second to determine if cross-coupling dynamics between the airframe and engine are of sufficient "magnitude" to significantly affect stability and/or performance of the feedback systems. The analysis technique also addresses the issue of the system's robustness against uncertainties in these interactions. Airframe/engine interactions are often a significant source of uncertainty in the system's dynamics.

Another objective of the paper is to use the analysis approach to evaluate airframe/engine cross-coupling on a vehicle that has been the subject of several studies in IFPC. The analysis reveals that critical cross-coupling is not present for this vehicle, as modeled, for the operating condition and control configuration evaluated. As a result, the classical control laws considered in this example would appear to deliver adequate stability robustness and performance. A second control configuration is then considered, and the analysis shows increased cross-coupling due to an added reaction control system (RCS) causing a significant degradation in engine loop performance.

Potential Sources of Airframe/Engine Interactions

The airframe/engine interactions highlighted in this section are elaborated on in Refs. 1–9. Consider for discussion purposes the vehicle system in Fig. 1. Thrust reversing nozzles may be considered for improving forward speed control of the aircraft. Vectoring of the engine's aft nozzle may be used to augment attitude control power, and ventral nozzle thrust may augment aerodynamic lift. Left and right ejectors, drawing primary thrust from the engine's mixed flow (core and bypass flow) and secondary thrust from intakes over the top of the fuselage may also augment lift and enhance pitch and roll control power. The lift and attitude responses of the airframe will be influenced by thrust disturbances in these sources, and effects of the ejector's secondary flow may significantly influence the airframe aerodynamics.

On the other hand, commands in thrust reversing, thrust vectoring, and ventral and ejector thrust may cause pressure disturbances in the augmentor or mixing plane. If the nozzle is operating in an unchoked condition, these pressure disturbances may propagate through the fan bypass duct and cause engine transients such as a reduction in fan surge margin.

Reaction control system jets, used for airframe attitude control, as well as upper wing surface blowing, used for lift augmentation, usually draw bleed air from the engine's compressor. Thus, core flow dynamics can also influence the lift and attitude responses of the airframe. Increased RCS thrust will cause reduced core pressure due to compressor bleed flow demand, creating engine flow disturbances. Also, flight dynamic pressure, angle of attack, sideslip angle, and inlet flow distortions can influence the effectiveness of the RCS control jets and cause reduced fan surge margin.

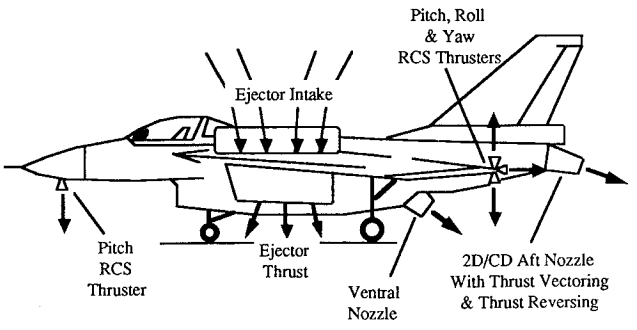

Fig. 1 Typical vehicle configuration.

Presented as Paper 90-1918 at the AIAA/SAE/ASME/ASEE 26th Joint Propulsion Conference, Orlando, FL, July 16–18, 1990; received Oct. 3, 1991; revision received Feb. 28, 1992; accepted for publication March 6, 1992.

*Research Associate and Doctoral Candidate, Aerospace Research Center, College of Engineering and Applied Sciences. Student Member AIAA.

†Professor of Engineering and Center Director, Aerospace Research Center, College of Engineering and Applied Sciences. Associate Fellow AIAA.

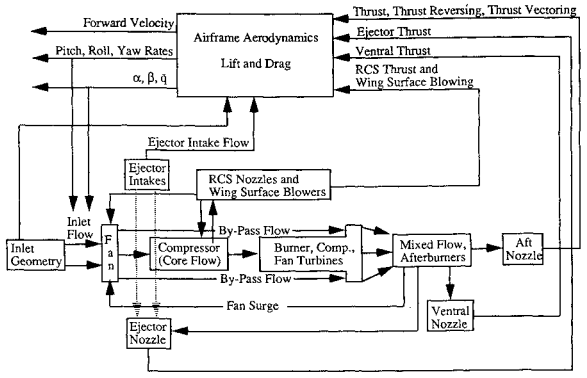

Fig. 2 Example interactions between airframe and engine subsystems.

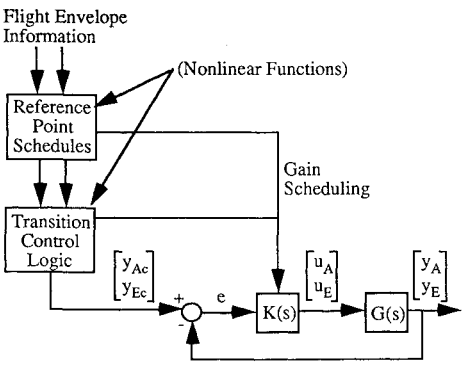

Fig. 3 Full nonlinear airframe/engine system representation.

It is important to note here that, for the type of vehicle being considered, the propulsion system not only affects the (slower responding) transitional velocity of the vehicle but also may be both a lift and moment "actuator," affecting the vehicle's (faster responding) attitude dynamics. All of these interactions just described between the airframe and engine are shown in Fig. 2.

Analysis Framework

The technique to be presented is a quasilinear approach for assessing airframe and engine interactions.[10] This procedure seeks to provide a better understanding of the effects of these interactions. It is recognized that many of the interactions discussed previously involve nonlinear phenomena, and detailed nonlinear simulations will ultimately be required. However, the justification for the quasilinear analysis and the treatment of engine limits is specifically noted herein.

Consider the airframe/engine nonlinear system similar to that discussed in Refs. 11–13 and shown in Fig. 3. y_{Ac} is the vector of commands to the flight control system, and y_{Ec} is the vector of commands to the engine control system. u_A is the vector of aircraft control inputs (flap deflection δ_F, thrust vector nozzle deflection δ_{TV}, etc.), and u_E is the vector of engine control inputs (fuel flow rate w_F, nozzle area A_7, etc.). Finally, y_A is the vector of aircraft responses (angle of attack α, pitch rate q, etc.), and y_E is the vector of engine responses (turbine temperature T_4, fan speed N_2, etc.).

Implicit in the feedback portion of this system is that the matrix $G(s)$, the quasilinear input/output mapping of the vehicular system, is a member of a set of such mappings, $\mathcal{G}(s)$, and strongly depends on the particular flight and engine operating condition. In fact, each such operating point manifests a particular quasilinear system model and control architecture, which define the matrices $G(s)$ and $K(s)$. Furthermore, these mappings may reflect a particular control mode, such as "riding an engine limit." In such a case, the controlled responses $y_E(s)$ depend on the operating limit. In the discussion to follow, it is implied that the analysis is being performed for a specific operating condition and a specific engine control mode.

If it can be assumed here that any gain scheduling leads to slowly time-varying gains, then the particular feedback system being considered can be treated as (approximately) time invariant. In this case, the system nonlinearities reside primarily outside the feedback loop, and the purpose of feedback is to force approximately linear behavior between $\bar{y}$ and $\bar{y}_c$. The analysis framework that follows focuses only on the feedback portion of the system. However, this does not imply that the prefilters, gain scheduling, limit logic, etc., outside the feedback loop are not important to the system design, but that stability and performance of the feedback loops are fundamental to a successful design. Furthermore, since the feedback control loops for the airframe and engine are, under current practice, developed by different organizations, it could be argued that interactions in these loops would constitute the most difficult design challenge.

Now, more specifically, consider the aircraft dynamics isolated from the engine dynamics, with input/output characteristics defined in terms of a matrix of transfer functions $G_A^*(s)$, where

$$y_A(s) = G_A^*(s)u_A(s) \tag{1}$$

Likewise, let the isolated engine's input/output characteristics be defined in terms of a matrix of transfer functions $G_E^*(s)$, where

$$y_E(s) = G_E^*(s)u_E(s) \tag{2}$$

Consider that each of these systems will be acted on by feedback control compensation matrices $K_A(s)$ for the aircraft flight control system, and $K_E(s)$ for the engine control system. The associated engine feedback system is shown in Fig. 4 [note again that $K_E(s)$ and $G_E^*(s)$ are, in general, matrices].

The closed-loop quasilinear responses of this system are given by

$$y_E(s) = \left[I + G_E^*(s)K_E(s)\right]^{-1} G_E^*(s)K_E(s)\,y_{Ec}(s) \tag{3}$$

and the closed-loop characteristic polynomial is

$$\phi_{cl}(s) = \phi_{ol}(s)\det\left[I + G_E^*(s)K_E(s)\right] \tag{4}$$

where the roots of $\phi_{ol}(s)$ are an aggregate of the poles of $G_E^*(s)$ and $K_E(s)$.

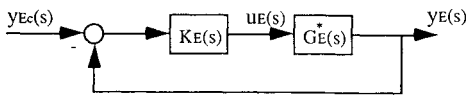

Fig. 4 Block diagram of the isolated engine feedback loop.

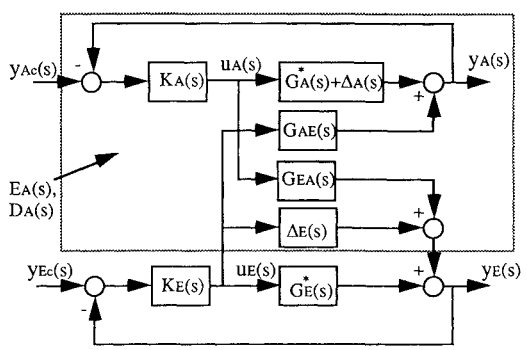

Fig. 5 Block diagram of the coupled airframe/engine system.

But since the airframe/engine system dynamics are in fact coupled, their input/output characteristics are more accurately represented as

$$\begin{bmatrix} y_A(s) \\ y_E(s) \end{bmatrix} = \begin{bmatrix} G_A(s) & G_{AE}(s) \\ G_{EA}(s) & G_E(s) \end{bmatrix} \begin{bmatrix} u_A(s) \\ u_E(s) \end{bmatrix} = [G(s)] \begin{bmatrix} u_A(s) \\ u_E(s) \end{bmatrix} \tag{5}$$

where, again, $G_A(s)$, $G_E(s)$, $G_{AE}(s)$, and $G_{EA}(s)$ are, in general, matrices. Note also that $G_A(s)$ and $G_E(s)$ may differ from the decoupled subsystem models $G_A^*(s)$ and $G_E^*(s)$ by some amounts $\Delta_A(s)$ and $\Delta_E(s)$, respectively, due to the cross-coupling actually present between the airframe and engine systems. That is,

$$\begin{aligned} G_A(s) &= G_A^*(s) + \Delta_A(s) \\ G_E(s) &= G_E^*(s) + \Delta_E(s) \end{aligned} \tag{6}$$

Further, $G_{AE}(s)$ and $G_{EA}(s)$ represent any input coupling that leads to the open-loop engine control inputs influencing airframe responses or the open-loop airframe control inputs influencing the engine responses, respectively. Now, if both $G_{AE}(s)$ and $G_{EA}(s)$ are "large," the system is said to exhibit two-directional coupling. If only one is "large," the coupling between the subsystems is primarily one-directional.

The actual coupled system, under the influence of the airframe and engine control feedback compensation $K_A(s)$ and $K_E(s)$, is then shown in Fig. 5. In this figure the lower portion of the block diagram is the original engine loop, but it is no longer isolated from the airframe as in Fig. 4.

Figure 5 reveals how, for example, the coupling dynamics $G_{AE}(s)$ and $G_{EA}(s)$ and the airframe dynamics $G_A(s)$, augmented with the airframe compensator $K_A(s)$, interact with the engine loops. (Note that a dual exists for the effects of the coupling and augmented engine dynamics on the airframe loops.) Through block diagram manipulation, the system in Fig. 5 may be represented as in Fig. 6, where

$$E_A(s) = \Delta_E - G_{EA}\left[I + K_A(G_A^* + \Delta_A)\right]^{-1} K_A G_{AE} \tag{7}$$

$$D_A(s) = G_{EA}\left[I + K_A(G_A^* + \Delta_A)\right]^{-1} K_A \tag{8}$$

(Note that functional dependence on s is not indicated in some of these terms to simplify notation.) Because of the manner in which these terms affect the engine loop, $E_A(s)$ will be referred to as the additive interaction matrix, and $D_A(s)$ will be referred to as the disturbance interaction matrix. Clearly, if $\Delta_A(s)$, $\Delta_E(s)$, $G_{AE}(s)$, and $G_{EA}(s)$ are not really zero, the engine loop is not actually that shown in Fig. 2 but rather that shown in Fig. 6

The critical expressions of Eqs. (7) and (8) reveal several key facts. First, Eq. (7) shows that the additive interaction matrix $E_A(s)$ depends on the weighted matrix product of the input coupling transfer matrices $G_{EA}(s)$ and $G_{AE}(s)$, the airframe dynamics $G_A^*(s) + \Delta_A(s)$, and the change in the engine transfer function matrix due to coupling $\Delta_E(s)$. $E_A(s)$ will therefore be "small" (for example, small maximum singular value) if Δ_E is "small" and if either $G_{AE}(s)$ or $G_{EA}(s)$ is "small." Thus, if only one-directional coupling is present, the additive interaction matrix will tend to be "small."

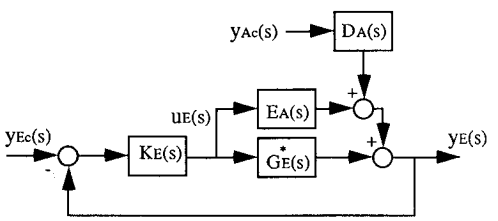

Fig. 6 Block diagram of the engine feedback loop interacting with the airframe subsystem.

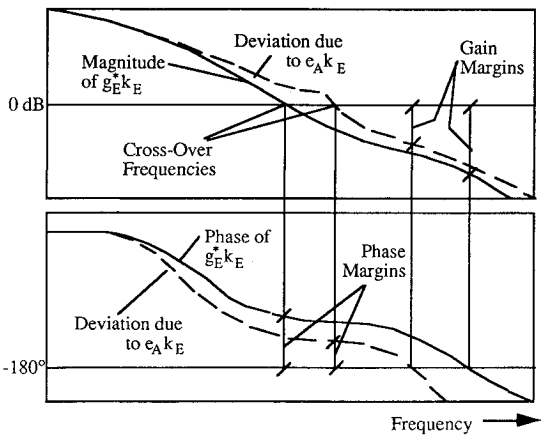

Fig. 7 Example noninteracting (solid line) and interacting (dashed line) systems' engine loop transfers.

Conversely, from Eq. (8), note that the disturbance interaction matrix $D_A(s)$ is independent of $G_{AE}(s)$. Hence, it may be "large" if $G_{EA}(s)$ is "large," even though $G_{AE}(s)$ is "small." That is, the disturbance interaction matrix can be "large" even if only one-directional coupling is present.

Finally, both the additive and disturbance interaction matrices depend explicitly on the airframe control laws $K_A(s)$. If the airframe loops are not closed [$K_A(s) = 0$], $E_A(s)$ reduces to $\Delta_E(s)$ and $D_A(s)$ reduces to zero. Consequently, the phenomenon of interest here is fundamentally one involving feedback.

To reveal the import of the additive and disturbance interaction matrices, note that the quasilinear responses of the engine system in Fig. 6 are

$$\begin{aligned} y_E(s) = &\left[I + (G_E^* + E_A)K_E\right]^{-1}(G_E^* + E_A)K_E y_{Ec}(s) \\ &+ \left[I + (G_E^* + E_A)K_E\right]^{-1} D_A y_{Ac}(s) \end{aligned} \tag{9}$$

Comparison of the decoupled engine system's input/output relationship of Eq. (3) with the truly coupled system's input/output relationship of Eq. (9) reveals that the additive interaction matrix $E_A(s)$ can affect both stability and performance of the engine feedback system. However, the disturbance interaction matrix $D_A(s)$ does not affect stability of the quasilinear system, since (as shown later) the characteristic polynomial of the closed-loop coupled system is independent of this matrix. Clearly, however, $D_A(s)$ has an impact on the engine control system performance. Commands into the flight control system $y_{Ac}(s)$ disturb the engine responses through $D_A(s)$ and appear as output disturbances to the engine control loops. Thus, if $D_A(s)$ is large, the closed-loop engine performance will suffer.

Quite significant is the fact that $E_A(s)$ can affect the interacting system's closed-loop stability. The closed-loop characteristic polynomial for the coupled system is

$$\phi_{cl}(s) = \phi_{ol}(s) \det\left\{I + \left[G_E^*(s) + E_A(s)\right]K_E(s)\right\} \tag{10}$$

Here the roots of $\phi_{ol}(s)$ are an aggregate of the poles of $K_E(s)$ and the poles of the system with only the airframe loops closed with $K_A(s)$, or the values of s for which $\det[I + G_A(s)K_A(s)] = 0$. These facts are derived in Appendix A. Now it can be shown from Nyquist stability theory[14] that the closed-loop system in Fig. 6 is assured to remain stable if the feedback loop is stable for $E_A(s) = 0$, and if

$$\det\left\{I + \left[G_E^*(j\omega) + \epsilon E_A(j\omega)\right]K_E(j\omega)\right\} \neq 0, \quad [0 < \epsilon < 1] \tag{11}$$

for all frequencies $\omega > 0$. It can further be shown that this is assured if

$$\bar{\sigma}\left[E_A(j\omega)K_E(j\omega)\right] < \underline{\sigma}\left[I + G_E^*(j\omega)K_E(j\omega)\right] \quad \text{for all } \omega > 0 \tag{12}$$

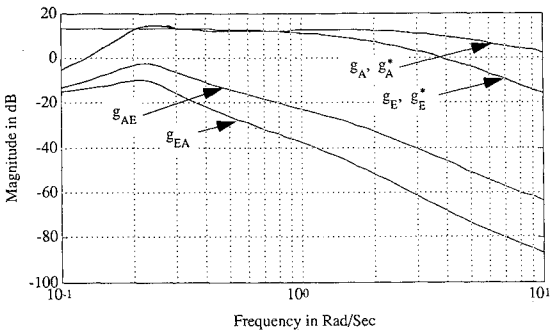

Fig. 8 Open-loop normalized transfer function magnitudes.

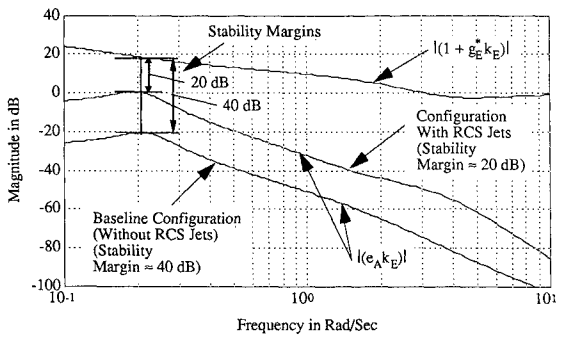

Fig. 9 Plot of Eq. (17), the scalar form of Eq. (12).

or if

$$\bar{\sigma}\left\{E_A(j\omega)\left[G_E^*(j\omega)\right]^{-1}\right\} < \underline{\sigma}\left\{I + \left[G_E^*(j\omega)K_E(j\omega)\right]^{-1}\right\} \quad \text{for all } \omega > 0 \tag{13}$$

where $\bar{\sigma}$ and $\underline{\sigma}$ denote the maximum and minimum singular values of a matrix, respectively.

These key inequalities are measures of the overall system's stability robustness with respect to uncertainties in airframe/engine interactions. In fact, the system's robustness can be indicated by plotting both sides of Eq. (12) or (13). It is evident that there will be loss of robustness at frequencies where $E_A(s)$ is "large" (i.e., if its maximum singular value is large). At these critical frequencies, a stability robustness margin may be defined as the distance between the left- and right-hand sides of Eq. (12) or (13). Since $E_A(s)$ is a strong function of the cross-coupling dynamics $G_{AE}(s)$ and $G_{EA}(s)$, small variations in elements of either $G_{AE}(s)$ or $G_{EA}(s)$ at some critical frequency may reduce this margin to zero and thus lead to the failure of the aforementioned stability criteria.

The significance of the preceding results may be seen more clearly by considering a single-input/single-output engine control system. Let the regulated engine response of interest be, for example, fan speed N_2, and, for a fixed nozzle area, let the control input be the main burner fuel flow rate w_F. In this case, the transfer function matrices $G_E^*(s)$, $\Delta_A(s)$, $K_E(s)$, and $E_A(s)$, as well as $D_A(s)$, reduce to scalars, denoted by $g_E^*(s)$, $\delta_A(s)$, $k_E(s)$, $e_A(s)$, and $d_A(s)$. Then Eq. (9) reduces to the scalar relationship

$$y_E(s) = \left[\frac{(g_E^* + e_A)k_E}{1 + (g_E^* + e_A)k_E}\right] y_{Ec} + \left[\frac{1}{1 + (g_E^* + e_A)k_E}\right] d_A y_{Ac} \tag{14}$$

Also, if all system transfer functions are assumed to be scalars, Eqs. (7) and (8) reduce to

$$e_A(s) = \delta_E - \frac{g_{EA} g_{AE} k_A}{1 + k_A(g_A^* + \delta_A)} \tag{15}$$

$$d_A(s) = \frac{g_{EA} k_A}{1 + k_A(g_A^* + \delta_A)} \tag{16}$$

Equation (15) shows clearly that $e_A(s)$ is a strong function of the frequency-dependent (weighted) product of $g_{EA}(s)$ and $g_{AE}(s)$. Hence, if either $g_{AE}(s)$ or $g_{EA}(s)$ (or both) are small and $\delta_E(s)$ is small at critical frequencies, then $e_A(s)$ will tend to be small at those frequencies.

The characteristic equations in Eq. (14) also show that if $e_A(s)$ is large, then gain and phase margins present in the decoupled engine loop transfer $[k_E(s)g_E^*(s)]$ may be eroded in the coupled engine loop transfer, as depicted in Fig. 7. However, from Eq. (12), stability of the coupled system is assured if

$$|e_A(j\omega)k_E(j\omega)| < |1 + g_E^*(j\omega)k_E(j\omega)| \quad \text{for all } \omega > 0 \tag{17}$$

which is the scalar form of Eq. (12).

Note that the focus of this analysis has been the effect of airframe dynamics on the engine loop. A dual analysis reveals how the interactions affect the airframe attitude loops. That is, the dual of Eq. (9) gives the airframe responses for the interacting system as

$$y_A(s) = \left[I + (G_A^* + E_E)K_A\right]^{-1}(G_A^* + E_E)K_A y_{Ac}(s) + \left[I + (G_A^* + E_E)K_A\right]^{-1} D_E y_{Ec}(s) \tag{18}$$

where the interaction matrices $E_E(s)$ and $D_E(s)$, given below, are the duals of $E_A(s)$ and $D_A(s)$:

$$E_E(s) = \Delta_A - G_{AE}\left[I + K_E(G_E^* + \Delta_E)\right]^{-1} K_E G_{EA} \tag{19}$$

$$D_E(s) = G_{EA}\left[I + K_E(G_E^* + \Delta_E)\right]^{-1} K_E \tag{20}$$

The airframe loops are assured to remain stable in the presence of interaction uncertainties as long as

$$\bar{\sigma}\left[E_E(j\omega)K_A(j\omega)\right] < \underline{\sigma}\left[I + G_A^*(j\omega)K_A(j\omega)\right] \quad \text{for all } \omega > 0 \tag{21}$$

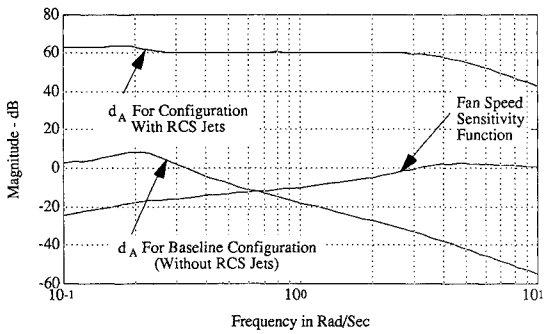

Fig. 10 Engine performance analysis.

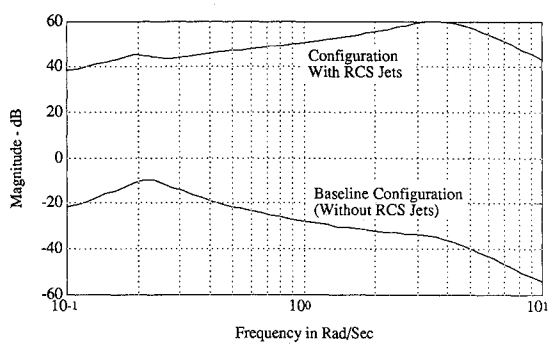

Fig. 11 Fan speed response from pilot pitch stick input (rpm/lb).

which is the dual of Eq. (12). Also, "large" $D_E(s)$, for example, will degrade the flying qualities of the flight control system due to disturbances arising from engine commands.

As a final note, this analysis does not necessarily require analytical models of the airframe and/or engine. Input/output mappings of the system could conceivably be experimentally obtained, and graphical data could be used exclusively to obtain plots of Eqs. (7), (8), and (12), for example.

Two Case Studies

The techniques just presented will now be used in the analysis of an airframe/engine system that has been the subject of several investigations of integrated flight and propulsion control.[1,3,4,14] The baseline vehicle to be considered is representative of a high-performance Short Takeoff and Landing (STOL) fighter aircraft equipped with a thrust-vectoring/thrust-reversing nozzle. The operating point under consideration is the approach-to-landing flight condition at an airspeed of $V_0 = 120$ kt and flight-path angle $\gamma_0 = -3$ deg. The quasilinear vehicle system model is that given in Refs. 10, 15, and 16. A second configuration will also be considered, which is identical to the baseline but with a high-pressure RCS added. Although significant airframe/engine coupling may be expected, the analysis will show that little critical interactions exist for the baseline configuration, and only one-directional coupling is present for the configuration that includes the RCS. Note also that, although the analysis herein involves only single-input/single-output systems, the last section presented a multivariable methodology and thus is not restricted to scalar systems.

For both cases the airframe's dynamics are aerodynamically unstable. The airframe flight control design objective is to stabilize the airframe's dynamics and obtain classical pitch rate and angle-of-attack responses from pilot pitch stick input δ_{stick}. The objective of the engine control law is to regulate the fan speed. The control laws for both cases are given in Appendix B.

Case 1

The open-loop system is described as

$$\begin{bmatrix} (K_{\delta\alpha}/K_{\delta q})\alpha + q \\ N_2 \end{bmatrix} = \begin{bmatrix} g_A(s) & g_{AE}(s) \\ g_{EA}(s) & g_E(s) \end{bmatrix} \begin{bmatrix} \delta_{\text{pitch}} \\ w_f \end{bmatrix} \tag{22}$$

where, for example,

$$g_A(s) = \frac{-14(s+0.03\pm0.07j)(s+0.6)(s+1.4)(s+3.6)(s+7)(s+90)}{(s+0.06\pm0.2j)(s+1.4)(s-1.5)(s+2)(s+3.6)(s+7)(s+90)}$$

$$g_E(s) = \frac{1.3(s+0.06\pm0.2j)(s-1.5)(s+2)(s+16\pm6j)(s+37)}{(s+0.06\pm0.2j)(s+1.4)(s-1.5)(s+2)(s+3.6)(s+7)(s+90)} \tag{23}$$

Note the unstable mode at 1.5 rad/s. From Appendix B, the control law is

$$\begin{bmatrix} \delta_{\text{pitch}} \\ w_f \end{bmatrix} = -\begin{bmatrix} K_{\delta q} & 0 \\ 0 & 6(s+\tfrac{1}{2})/s \end{bmatrix} \begin{bmatrix} (K_{\delta\alpha}/K_{\delta q})\alpha + q \\ N_2 \end{bmatrix} - \begin{bmatrix} K_{\delta\text{st}}/K_{\delta q} \\ 0 \end{bmatrix} \delta_{\text{stick}} \tag{24}$$

where w_f = fuel flow rate, and the pitch attitude control δ_{pitch}, the feedback gains $K_{\delta\alpha}$ and $K_{\delta q}$, and the pilot stick gain $K_{\delta\text{st}}$ are given in Appendix B. These control laws lead to gain crossover frequencies in the engine and aircraft pitch loops of approximately 3 and 5 rad/s, respectively.

Shown in Fig. 8 are the magnitudes of the input/output mappings in Eq. (22), as well as the mappings for the decoupled airframe and engine $g_A^*(s)$ and $g_E^*(s)$. To properly evaluate the relative sizes of the input/output relationships of the airframe and engine, the system must be normalized by, for example, estimates of the maximum values of the controls and responses. The values used to normalize this plant are given in Table 1 and are taken from Ref. 9.

Figure 8 reveals that the cross-coupling terms $g_{AE}(s)$ and $g_{EA}(s)$ are both smaller than the diagonal elements in Eq. (22) by approximately 40 dB for frequencies above 1 rad/s. (Recall that the loop gain cross-over frequencies are around 3-5 rad/s.) Also, since there are no visible differences in the plots of $g_A(s)$ and $g_A^*(s)$, and $g_E(s)$ and $g_E^*(s)$, $\Delta_A(s)$ and $\Delta_E(s)$ are quite small. Hence, from Eqs. (7), (8), (19), and (20), $e_A(s)$, $d_A(s)$, $e_E(s)$, and $d_E(s)$ should all be quite small, and it might be expected that airframe/engine interactions will be negligible. However, the complete analysis requires knowledge of candidate control laws, since feedback compensation could increase critical cross-coupling.

Shown in Fig. 9 are plots of both sides of the key inequality of the stability robustness analysis, Eq. (12) or (17). This figure shows that $|e_A k_E|$ for the baseline configuration is much less than $|1 + g_E^* k_E|$ throughout the frequency range shown. The stability margin, defined here as the minimum distance between the left- and right-hand sides of the inequality of Eq. (12) or (17), occurs near 0.2 rad/s and is approximately 40 dB for the baseline configuration. Therefore, the analysis indicates significant engine loop stability robustness against uncertainties in airframe/engine interactions.

Figure 10 presents the magnitude of the engine's fan speed sensitivity function $\{1/[1 + (g_E + e_A)k_E]\}$ along with the magnitude of the engine loop disturbance interaction due to pilot input $d_A(j\omega)$ [Eq. (8) or (16)] for the baseline configuration. The spectrum of the engine response because of these disturbances, or $N_2/\delta_{\text{stick}}$, is shown in Fig. 11, also labeled as the baseline configuration. This response is, of course, the product of the two terms plotted in Fig. 10. These plots reveal that the fan speed loop will reject disturbances arising from pilot pitch inputs, since $g_{EA}(j\omega)$ is small.

In summary, the analysis of this airframe/engine system description indicates that the additive and disturbance interaction effects $e_A(s)$ and $d_A(s)$ are small [and although not shown, $e_E(s)$ and $d_E(s)$ are small as well]. Hence, the coupling in this vehicle will not significantly degrade the closed-loop performance of both the airframe and engine subsystems; the system is therefore robust against interaction uncertainties and decentralized control laws appear quite adequate.

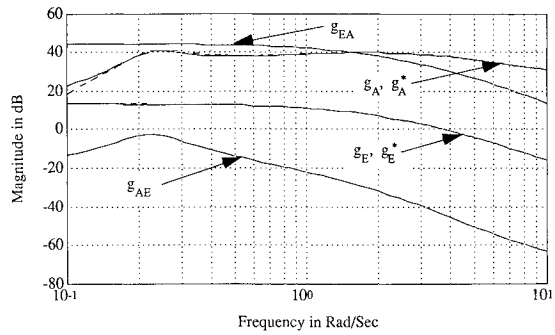

Fig. 12 Open-loop normalized transfer function magnitudes with pitch RCS control included.

Table 1 Estimates of maximum values of controls and responses

$q_{max} = 0.06$ rad/s
$\alpha_{max} = 3$ deg
$N_{2\,max} = 570$ rpm
$\delta_{TV\,max} = 10$ deg
$w_{f\,max} = 5000$ lb/h

Table 2 Additive perturbations of $g_{AE}(j\omega)$

Case	$\delta\lvert g_{AE}\rvert$, (rad/s)/(lb/h)
1	1.6
2	3.2
3	4.7
4	6.3
5	6.7

over the frequency range shown. Hence, strong one-directional coupling is indicated.

The large increase in the magnitude of $g_{EA}(j\omega)$ causes the magnitude of $d_A(j\omega)$ to significantly increase [see Eq. (16)], as shown in Fig. 10. This figure indicates that the engine loop can no longer effectively reject fan speed disturbances arising from pilot pitch stick inputs. In fact, Fig. 11 shows the significant increase in the magnitude of the fan speed response due to pilot pitch stick input over the baseline case.

Furthermore, the increase in magnitude of $g_{EA}(j\omega)$ causes an increase in magnitude of $e_A(j\omega)$ over the baseline configuration as well, as indicated in Fig. 9. Hence, stability robustness against uncertainties in airframe/engine interactions is reduced. Figure 9 shows that the stability margin is reduced from the baseline configuration to approximately 20 dB, again measured at 0.2 rad/s. It is worth noting that this critical frequency is well removed from the cross-over frequencies of the airframe and engine loops (3 and 5 rad/s). Note that in this situation small increases in the magnitude of $g_{AE}(j\omega)$ may cause a substantial increase in the additive interaction term $e_A(j\omega)$, since this term is a strong function of the product of $g_{AE}(j\omega)$ and $g_{EA}(j\omega)$ [Eq. (15)]. Hence, small variations in $g_{AE}(j\omega)$ may therefore cause significant degradation in stability robustness and/or performance. For these reasons, a sensitivity study will be performed on $g_{AE}(j\omega)$.

For this vehicle and control system configuration, the pitch trim occurs at a small thrust-vectoring angle δ_{TV}. Thus, engine

The airframe/engine system's closed-loop airframe transfer functions [see Eq. (18)] are

$$\alpha(s) = \frac{-0.1(s+0.06\pm0.2j)(s+30)}{(s+0.05\pm0.2j)(s+2.8\pm2.8j)}\,T_1(s)\left(\frac{\text{deg}}{\text{lb}}\right)\delta_{stick}(s) + \frac{-4e-4(s+2\pm0.6j)(s+4)(s+5)(s-76)}{(s+0.05\pm0.2j)(s+2.8\pm2.8j)}\,T_2(s)\left(\frac{\text{deg}}{\text{rpm}}\right)N_{2c}(s)$$

$$q(s) = \frac{-0.05s(s+0.07)(s+0.5)}{(s+0.05\pm0.2j)(s+2.8\pm2.8j)}\,T_1(s)\left(\frac{\text{rad/s}}{\text{lb}}\right)\delta_{stick}(s) + \frac{-4e-5(s+2)(s+3)(s+7\pm2j)(s-21)}{(s+0.05\pm0.2j)(s+2.8\pm2.8j)}\,T_2(s)\left(\frac{\text{rad/s}}{\text{rpm}}\right)N_{2c}(s)$$

where

$$T_1(s) = \frac{(s+0.4)(s+2\pm4j)(s+8)(s+90)}{(s+0.4)(s+2\pm4j)(s+8)(s+90)} \qquad T_2(s) = \frac{s}{(s+0.4)(s+2\pm4j)(s+8)(s+90)} \tag{25}$$

and where $T_1(s)$ is unity to the accuracy displayed, indicating that engine modes are essentially unobservable in the airframe responses. The transfer functions between the airframe responses and commanded fan speed N_{2c} are also quite small since the disturbance interaction effect $d_E(s)$ is small.

The closed-loop fan speed response [see Eq. (9) or (14)] for the airframe/engine system is

$$N_2(s) = \frac{-(s-2)(s+4\pm2j)(s+90)}{(s+0.4)(s+2\pm4j)(s+8)(s+90)}\,T_1(s)\left(\frac{\text{rpm}}{\text{rpm}}\right)N_{2c}(s) + \frac{-0.06(s-6)(s+7)(s-258)}{(s+0.4)(s+2\pm4j)(s+8)(s+90)}\,T_2(s)\left(\frac{\text{rpm}}{\text{lb}}\right)\delta_{stick}(s)$$

where

$$T_1(s) = \frac{(s+0.05\pm0.2j)(s+2.8\pm2.8j)}{(s+0.05\pm0.2j)(s+2.8\pm2.8j)} \qquad T_2(s) = \frac{s(s+0.4)(s+3\pm2j)}{(s+0.05\pm0.2j)(s+2.8\pm2.8j)} \tag{26}$$

As with the airframe responses, $T_1(s)$ is unity, indicating that airframe modes are essentially unobservable in the engine response. The fan speed response from pilot pitch stick input is quite small since $d_A(s)$ is small.

Case 2

Now consider the same vehicle with similar control laws but with pitch attitude control power enhanced by a combination of thrust vectoring and pitch RCS jets. RCS jets, which draw bleed flow from the engine's compressor, will directly influence the quality of airflow through the engine, thus increasing airframe/engine interactions. Models of the effects of bleed flow on the propulsion system were provided by the NASA Lewis Research Center. The control laws for this configuration are also detailed in Appendix B and are such that the airframe and engine control loops, cross-over frequencies, etc., are essentially the same as those for the baseline configuration.

The magnitudes of the elements of the plant transfer function matrix [Eq. (22)] are shown in Fig. 12. Again, the plant was normalized using the maximum values of control inputs and responses given in Table 1, and the maximum value of the pitch RCS jet nozzle area A_q was 1 in.^{2}. When compared with Fig. 8, this figure shows that the addition of pitch RCS control increases the magnitude of $g_{EA}(j\omega)$ by approximately 50 dB

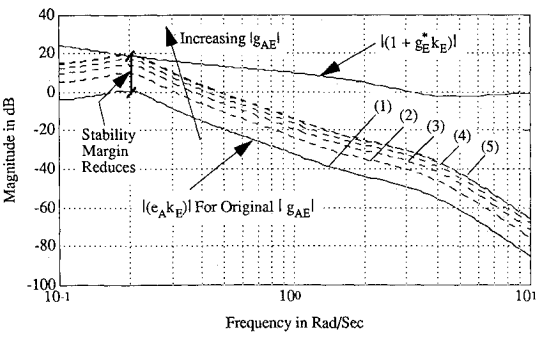

Fig. 13 Plot of Eq. (17) for various magnitudes of engine-to-airframe interactions, $|g_{AE}(j\omega)|$.

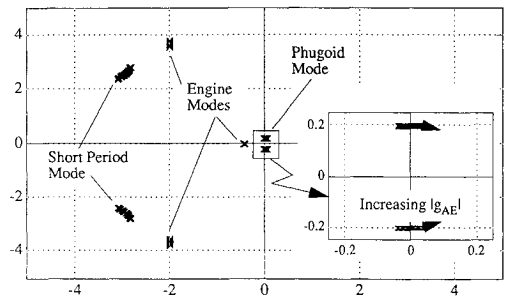

Fig. 14 Locus of the airframe/engine system's closed-loop poles as the magnitude of $g_{AE}(j\omega)$ is increased.

thrust transients will not generate large pitching moments, and this is the reason $g_{AE}(s)$ is small in this case. If the vehicle configuration was such that the trim thrust-vectoring angle were large, thus increasing the component of the thrust vector perpendicular to the airframe's longitudinal axis, engine thrust transients would create larger pitching moments. In such a case, $g_{AE}(s)$ would be larger.

Figure 13, like Fig. 9, shows the inequality of Eq. (17). This figure, however, displays $|e_A k_E|$ for various values of the magnitude of $g_{AE}(j\omega)$. Here,

$$g_{AE}(j\omega) = \left(|g_{AE}|_{\text{nominal}} + \delta|g_{AE}|\right) e^{j\phi_{AE}} \tag{27}$$

Table 2 lists the additive perturbations of the magnitude of $g_{AE}(j\omega)$ corresponding to the dashed curves in Fig. 13.

Figure 13 shows that $|e_A k_E|$ is much less than $|1+g_E k_E|$ throughout the frequency range for the nominal magnitude of $g_{AE}(j\omega)$, and stability of the system is not in jeopardy. However, the stability margin reduces to zero ($|e_A k_E| = |1+g_E^* k_E|$) at ≈ 0.2 rad/s when the magnitude of $g_{AE}(j\omega)$ is increased by only 6.7 (rad/s)/(lb/h) (case 5). From Fig. 12, note that $g_{AE}(j\omega)$, thus increased, would become comparable in magnitude to the other transfer functions in the system.

Figure 14 shows how the closed-loop eigenvalues of the system vary as the magnitude of $g_{AE}(j\omega)$ is increased. Higher frequency engine poles are not shown and do not vary to any great extent. However, this figure shows that a low-frequency (phugoid mode) instability does indeed occur at a frequency of 0.2 rad/s. Further, this instability occurs precisely for the increase in magnitude of $g_{AE}(j\omega)$ corresponding to case 5 in Fig. 13. It is also significant that the critical frequency of instability (0.2 rad/s) is not near the engine or airframe loop cross-over frequencies where phase margin is measured and that Eq. (17) correctly indicated that instability will first occur at this critical frequency due to variations in airframe/engine interactions.

Conclusions

Expressions were derived for additive and disturbance interaction matrices that may be used to quantify the significance of airframe/engine interactions on either the engine control loops or, for the dual analysis, the flight control loops. A technique for determining the stability robustness of the system against uncertainties in these interactions was presented. The size of the interaction matrices in critical frequency ranges, measured, for example, by their singular values, quantifies the effect of airframe/engine coupling on closed-loop stability and/or performance. The critical interaction matrices were shown to depend on the control compensation as well as the input/output characteristics of the airframe/engine system. If the system exhibits two-directional coupling, stability as well as performance may be compromised. Systems with one-directional coupling may preserve adequate stability robustness, although performance can be seriously affected.

This analysis was then applied to an airframe/engine system considered in previous integrated control studies, and two cases were presented. The baseline configuration was shown to exhibit few interactions. Classical decentralized control laws therefore appear quite suitable. However, the analysis revealed significant one-directional cross-coupling for a second control configuration with a reaction control system added. Inclusion of the RCS jets led to significant disturbances in the fan speed loop arising from pilot pitch inputs, and reduction in the stability robustness against variations in airframe/engine interactions was also recorded. The analysis accurately indicated the frequency at which instability would first occur due to these variations. Frequently, only engine-to-airframe interactions are thought to be of concern; however, this case clearly indicates strong airframe-to-engine coupling. In some previous IFPC studies only engine-to-airframe interactions were thought to be of concern. Although this may have been a valid assumption for the vehicle configurations examined, analysis methodologies should, in general, consider two-directional coupling.

Appendix A: Derivation of Eq. (10)

Let a state-space realization of the input/output mapping for the fully coupled aircraft/engine system be defined as

$$\begin{bmatrix}\dot{x}_A\\ \dot{x}_E\end{bmatrix} = \begin{bmatrix}A_A & A_{AE}\\ A_{EA} & A_E\end{bmatrix}\begin{bmatrix}x_A\\ x_E\end{bmatrix} + \begin{bmatrix}B_A & B_{AE}\\ B_{EA} & B_E\end{bmatrix}\begin{bmatrix}u_A\\ u_E\end{bmatrix}$$
$$\begin{bmatrix}y_A\\ y_E\end{bmatrix} = \begin{bmatrix}C_A & 0\\ 0 & C_E\end{bmatrix}\begin{bmatrix}x_A\\ x_E\end{bmatrix} \tag{A1}$$

and the mapping given as

$$\begin{bmatrix}y_A(s)\\ y_E(s)\end{bmatrix} = \begin{bmatrix}G_A(s) & G_{AE}(s)\\ G_{EA}(s) & G_E(s)\end{bmatrix}\begin{bmatrix}u_A(s)\\ u_E(s)\end{bmatrix} = [G(s)]\begin{bmatrix}u_A(s)\\ u_E(s)\end{bmatrix} \tag{A2}$$

with system characteristic polynomial

$$\phi_S(s) = \det\begin{bmatrix}sI-A_A & -A_{AE}\\ -A_{EA} & sI-A_E\end{bmatrix} \tag{A3}$$

Also let the state-space descriptions of the aircraft and engine compensation $K_A(s)$ and $K_E(s)$ be, respectively,

$$\dot{x}_{k_A} = A_{k_A}x_{k_A} + B_{k_A}\epsilon_{Ac}, \qquad u_A = C_{k_A}x_{k_A}$$
$$\dot{x}_{k_E} = A_{k_E}x_{k_E} + B_{k_E}\epsilon_{Ec}, \qquad u_E = C_{k_E}x_{k_E} \tag{A4}$$

where $\epsilon_{Ac}(s) = y_{Ac}(s) - y_A(s)$ and $\epsilon_{Ec}(s) = y_{Ec}(s) - y_E(s)$ are the inputs to the aircraft and engine compensators. The characteristic polynomials of these compensators are

$$\phi_{k_A}(s) = \det(sI - A_{k_A})$$
$$\phi_{k_E}(s) = \det(sI - A_{k_E}) \tag{A5}$$

Sought now is the state-space description of $G_E^*(s) + E_A(s)$, as presented in Fig. 6. Using Eqs. (A1) and (A4), and referring to Fig. 5, yields the desired result, or

$$\begin{bmatrix}\dot{x}_A\\ \dot{x}_E\\ \dot{x}_{k_A}\end{bmatrix} = \begin{bmatrix}A_A & A_{AE} & B_A C_{k_A}\\ A_{EA} & A_E & B_{EA}C_{k_A}\\ -B_{k_A}C_A & 0 & A_{k_A}\end{bmatrix}\begin{bmatrix}x_A\\ x_E\\ x_{k_A}\end{bmatrix}$$
$$+ \begin{bmatrix}B_{AE}\\ B_E\\ 0\end{bmatrix}u_E + \begin{bmatrix}0\\ 0\\ B_{k_A}\end{bmatrix}y_{Ac}$$
$$y_E = [0 \quad C_E \quad 0]\begin{bmatrix}x_A\\ x_E\\ x_{k_A}\end{bmatrix} \tag{A6}$$

Denoting this system as

$$\dot{x}_1 = A_1 x_1 + B_1 u_E + B_2 y_{Ac}$$
$$y_E = C_1 x_1 \tag{A7}$$

it can be shown[17] that the characteristic polynomial of this system $[G_E^*(s) + E_A(s)]$ is

$$\phi_1(s) = \det(sI - A_1) = \phi_S(s)\phi_{k_A}(s) \det\left[I + G_A(s)K_A(s)\right] \tag{A8}$$

Appending the state equation for the engine compensator $K_E(s)$ to the state equation for $G_E^*(s) + E_A(s)$ gives the state-space description of the open-loop system of Fig. 6 {or $[G_E^*(s) + E_A(s)]K_E(s)$} as

$$\begin{bmatrix} \dot{x}_1 \\ \dot{x}_{k_E} \end{bmatrix} = \begin{bmatrix} A_1 & B_1 C_{k_E} \\ 0 & A_{k_E} \end{bmatrix} \begin{bmatrix} x_1 \\ x_{k_E} \end{bmatrix} + \begin{bmatrix} 0 \\ B_{k_E} \end{bmatrix} \epsilon_{Ec} + \begin{bmatrix} B_2 \\ 0 \end{bmatrix} y_{Ac}$$
$$y_E = [C_1 \quad 0] \begin{bmatrix} x_1 \\ x_{k_E} \end{bmatrix} \tag{A9}$$

The characteristic polynomial of this system is

$$\phi_2(s) = \det \begin{bmatrix} sI - A_1 & -B_1 C_{k_E} \\ 0 & sI - A_{k_E} \end{bmatrix} = \phi_1(s)\phi_{k_E}(s) \tag{A10}$$

Closing the (engine) loop in Fig. 6, the state-space equation for the entire closed-loop system is then

$$\begin{bmatrix} \dot{x}_1 \\ \dot{x}_{k_E} \end{bmatrix} = \begin{bmatrix} A_1 & B_1 C_{k_E} \\ -B_{k_E} C_1 & A_{k_E} \end{bmatrix} \begin{bmatrix} x_1 \\ x_{k_E} \end{bmatrix} + \begin{bmatrix} 0 \\ B_{k_E} \end{bmatrix} y_{Ec} + \begin{bmatrix} B_2 \\ 0 \end{bmatrix} y_{Ac}$$
$$y_E = [C_1 \quad 0] \begin{bmatrix} x_1 \\ x_{k_E} \end{bmatrix} \tag{A11}$$

and the characteristic polynomial for this closed-loop system is

$$\phi_{cl}(s) = \det \begin{bmatrix} sI - A_1 & -B_1 C_{k_E} \\ B_{k_E} C_1 & sI - A_{k_E} \end{bmatrix}$$
$$= \phi_1(s)\phi_{k_E}(s) \det\left[I + (G_E^* + E_A)K_E\right] \tag{A12}$$

or

$$\phi_{cl}(s) = \phi_S(s)\phi_{k_A}(s) \det\left[I + G_A(s)K_A(s)\right]$$
$$\times \phi_{k_E}(s) \det\left[I + (G_E^* + E_A)K_E\right] \tag{A13}$$

Defining

$$\phi_{ol}(s) = \phi_S(s)\phi_{k_A}(s) \det\left[I + G_A(s)K_A(s)\right]\phi_{k_E}(s) \tag{A14}$$

gives

$$\phi_{cl}(s) = \phi_{ol}(s) \det\left[I + (G_E^* + E_A)K_E\right] \tag{A15}$$

which is the result presented as Eq. (10). Note that $\det[I + G_A(s)K_A(s)]$ is a rational function with denominator equal to $\phi_S(s)\phi_{k_A}(s)$. Thus, the roots of $\phi_{ol}(s)$ are the roots of $\phi_{k_E}(s)$, which are the poles of $K_E(s)$, and the values of s for which $\det[I + G_A(s)K_A(s)]$ equals zero.

Appendix B: Case Study Control Laws

The following defines the controls and measured responses for the case study vehicular system used in the analysis.

The aircraft control inputs are: δ_{TV} = nozzle thrust-vectoring angle, deg; A_q = pitch RCS jet nozzle area, in.^{2}; and δ_{flaps} = trailing-edge/leading-edge flap deflection angle, in.^{2}.

Table B1 Airframe control law gains

Gain	$\delta_{pitch} = \delta_{TV}$	$\delta_{pitch} = \delta_{TV} - 8A_q$
$K_{f\alpha}$, deg/deg	−2.9	−4.6
$K_{\delta\alpha}$, deg/deg	−3.7	−0.1
$K_{\delta q}$, deg/rad/s	−56.5	−2.3
$K_{\delta st}$, deg/lb	−0.7	−0.5

The engine control input is w_f = main burner fuel flow rate, lb/h.

The aircraft responses are α = angle of attack, deg, and q = pitch rate, rad/s.

The engine response is N_2 = engine fan speed, rpm.

Two cases are presented with different control architectures for pitch attitude control, defined as δ_{pitch}. For the first case, pitch is controlled only by thrust vectoring, thus, $\delta_{pitch} = \delta_{TV}$. For the second case, pitch is controlled by a "blend" of both thrust vectoring and pitch RCS jet nozzle area, defined as $\delta_{pitch} = \delta_{TV} - 8A_q$.

The airframe's short period mode is unstable, and the control objective is to stabilize the short period mode and obtain a desired modal frequency near 4 rad/s and a damping ratio of 0.7. This is achieved by feeding back angle of attack and pitch rate to pitch control. The other airframe control objective is to increase the flight-path time constant (usually denoted as $1/\tau_{\theta 2}$) to approximately 0.5 rad/s. This is achieved by feeding back angle of attack to the flaps. Finally, the pilot stick force gain is adjusted to give an approximate Bode gain on $q(s)/\delta_{stick}(s)$ of 0.03 (rad/s)/lb. In summary, the airframe control laws are

$$\delta_{flaps} = -K_{f\alpha}\alpha$$
$$\delta_{pitch} = -K_{\delta\alpha}\alpha - K_{\delta q}q - K_{\delta st}\delta_{stick} \tag{B1}$$

The values of the gains for both pitch control case are given in Table B1. Note that increased control power in using RCS jets led to the reduced feedback gains.

Finally, to regulate fan speed, fan speed is fed back through proportional plus integral compensation, with gains of −6 (lb/h)/rpm and −3 [(lb/h)s]/rpm, respectively.

The effects on system stability of the low gain flap loop are minimal. Therefore, the two-by-two system shown in Eq. (22) is obtained by first closing the flap loop and then combining the two aircraft attitude responses (α and q) to form one blended aircraft response.

Acknowledgments

This work was sponsored by the NASA Lewis Research Center under Grant NAG3-998. Peter Ouzts and Sanjay Garg have served as technical program managers.

References

[1]Smith, K., and Stewart, C., "A Survey of Control Law Options for Integrated Flight/Propulsion Control for Fighter STOL Approach," *Proceedings of the AIAA Guidance and Control Conference* (Seattle, WA), AIAA, New York, 1984 (AIAA Paper 84-1900).

[2]Shaw, P., Blumberg, K., Joshi, D., Anex, R., Vincent, J., and Skira, C., "Development and Evaluation of an Integrated Flight and Propulsion Control System," *Proceedings of the AIAA Joint Propulsion Conference* (Monterey, CA), AIAA, New York, 1985 (AIAA Paper 85-1423).

[3]Smith, K. L., "Design Methods for Integrated Control Systems," Aero Propulsion Lab., Air Force Wright Aeronautical Laboratories, AFWAL-TR-86-2103, Dayton, OH, Dec. 1986.

[4]Rock, S. M., Emami-Naeini, A., and Anex, R. P., "Propulsion Control Specifications in Integrated Flight/Propulsion Control Systems," *Proceedings of the AIAA/ASME/SAE/ASEE 24th Joint Propulsion Conference* (Boston, MA), AIAA, Washington, DC, 1988

(AIAA Paper 88-3236).

[5]Shaw, P. D., Rock, S. M., and Fisk, W. S., "Design Methods for Integrated Control Systems," Aero Propulsion Lab., Air Force Wright Aeronautical Laboratories, AFWAL-TR-88-2061, Dayton, OH, June 1988.

[6]Garg, S., Mattern, D. L., and Bullard, R. E., "Integrated Flight/Propulsion Control System Design Based on a Centralized Approach, *Proceedings of the AIAA Guidance, Navigation, and Control Conference* (Boston, MA), AIAA, Washington, DC, 1989 (AIAA Paper 89-3520).

[7]Berry, D., and Schweikhard, W., "Potential Benefits of Propulsion and Flight Control Integration for Supersonic Cruise Vehicles," based on SAE Paper 740478, 1974.

[8]Tape, R., Hartill, W., et al., "Vectoring Exhaust Systems for STOL Tactical Aircraft," *Journal of Engineering for Power, Transactions of the American Society of Mechanical Engineers,* July 1983.

[9]Garg, S., Mattern, D., Bright, M., and Ouzts, P., "*H*-Infinity Based Integrated Flight/Propulsion Control Design for a STOVL Aircraft in Transition Flight," NASA TM 103198, Aug. 1990.

[10]Schmidt, D., Schierman, J., and Garg, S., "Analysis of Airframe/Engine Interactions—An Integrated Control Perspective," *Proceedings of the AIAA/ASME/SAE/ASEE 26th Joint Propulsion Conference* (Orlando, FL), AIAA, Washington, DC, 1991 (AIAA Paper 90-1918).

[11]Peczkowski, J., and Stopher, S., "Nonlinear Multivariable Synthesis with Transfer Functions," *Proceedings of the 1980 Joint Automatic Control Conference,* Vol. 1, Pt. WA8-D, 1980.

[12]Sain, M., and Peczkowski, J., "Nonlinear Multivariable Design by Total Synthesis," Dept. of Electrical Engineering, Univ. of Notre Dame, Control System Technical Rept. 36, Notre Dame, IN, March 1985.

[13]Schmidt, D., and Schierman, J., "A Framework for the Analysis of Airframe/Engine Interactions and Integrated Flight/Propulsion Control," *Proceedings of the American Control Conference* (Boston, MA), June 1991, pp. 761–766.

[14]Doyle, J., and Stein, G., "Multivariable Feedback Design: Concepts for a Classical/Modern Synthesis," *IEEE Transactions on Automatic Control,* Vol. AC-26, No. 1, 1981, pp. 4–16.

[15]Schmidt, D., and Schierman, J., "Extended Implicit Model Following as Applied to Integrated Flight and Propulsion Control," *Proceedings of the AIAA Guidance, Navigation, and Control Conference* (Portland, OR), AIAA, Washington, DC, 1990 (AIAA Paper 90-3444).

[16]Schierman, J., and Schmidt, D., "Robust Control Synthesis for Integrated Flight and Propulsion Control," IEEE Conference on Decision and Control, Honolulu, HI, Dec. 1990.

[17]Kwakernaak, H., and Sivan, R., *Linear Optimal Control Systems,* Wiley-Interscience, New York, 1972.